Research articles

Static and dynamic energy losses along different directions in GO steel sheets

Carlo Appino[a,*], Enzo Ferrara[a], Fausto Fiorillo[a], Carlo Ragusa[b], Olivier de la Barrière[c]

[a] *Istituto Nazionale di Ricerca Metrologica (INRIM), Advanced Materials Metrology and Life Science, Torino, Italy*
[b] *Politecnico di Torino, Department of Energy, Torino, Italy*
[c] *Laboratoire SATIE, CNRS-ENS, Cachan, France*

A B S T R A C T

Grain-oriented (GO) Fe-Si sheets are often preferred to non-oriented steels in large rotating machines, where the material response along directions different from the rolling one (RD) matters, both in terms of magnetisation curve and energy losses. The experiments show that the material properties depend in a complex fashion on the angle θ made by the applied field with respect to RD in the lamination plane, an effect that can be quantitatively interpreted in terms of evolution of the domain wall processes. It was shown that the pre-emptive knowledge of the material behaviour along RD ($\theta = 0°$) and the transverse direction TD ($\theta = 90°$) allows one to predict, under quasi-static excitation, the normal magnetisation curve, the hysteresis loop shape, and the energy loss dependence on θ in high-permeability GO sheets. The evolution of the quasi-static magnetic properties with θ has an obvious counterpart in the dynamic behaviour. In the present work we have therefore investigated, from the experimental and theoretical viewpoint, the behaviour of the magnetic energy loss $W(f, J_p)$ versus frequency (1 Hz $\leqslant f \leqslant$ 200 Hz) and peak polarisation (0.15 T$\leqslant J_p \leqslant$ 1.6 T) in high-permeability 0.29 mm thick GO Epstein samples, cut at 15° steps between RD and TD. We show that the predicting method developed for the quasi-static loss can be made general through loss decomposition and applied, in particular, to the determination of the excess loss term. This leads to a general description of $W(f, J_p)$ as a function of the sheet cutting angle, without using arbitrary parameters.

1. Introduction

The appraisal of the magnetic properties of grain-oriented Fe-Si laminations [1] subjected to generically directed field comes strongly into play when dealing with applications (T-joints of transformers [2,3], and large rotating machines [4,5]). But the behaviour of the GO sheet along directions different from RD, essential for machine designers, cannot be retrieved from the data sheets, which deal with the performance of laminations cut along RD only (and are often limited to f = 50 Hz).

Insight into this problem, which has attracted modelling by means of static [6–8] and dynamic [9] formal approaches to magnetisation process and energy loss, and detailed investigations of the domain structure evolution [10–12], finds useful simplification and solid reference in the analysis of the single crystal behaviour. This approach permits one to investigate the intrinsic magnetic properties of the material from the analysis of its behaviour along the high-symmetry reference directions [0 0 1] and [1 1̄ 0], placing it in the framework of the

Néel Phase Theory [13], with due consideration of the role played by the demagnetising field [14].

When moving from this idealised scenario to the GO laminations, the reference directions become RD and TD, in place of [0 0 1] and [1 1̄ 0]. As a consequence, an important line of research is devoted to the problem of providing physical meaning to the prediction of the magnetic properties at intermediate directions starting from the knowledge of the response along RD and TD. A general drawback of the literature on this subject lies, however, on the prevalence of empirical methods, in combination with a certain neglect of the fundamental role played by the geometrical properties of the sample sheet [11,15–18].

In this paper, we discuss an experimental investigation on the behaviour of the energy loss W vs. f and J_p (the polarisation measured along the magnetising field direction) on Epstein strips cut at different angles θ to RD from a high permeability Goss-textured parent sheet (see left side of Fig. 1). Starting from a quasi-static model of the magnetisation process [14,19], we have developed a theoretical approach, relying on the loss separation procedure [20], by which one can
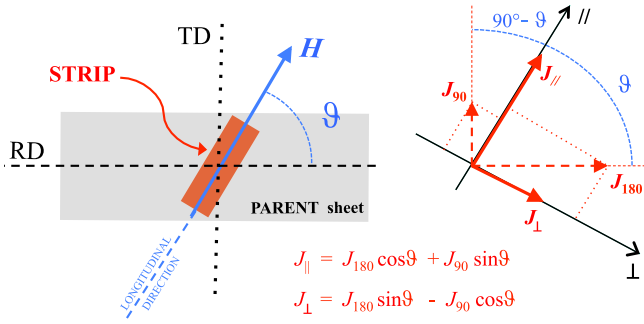
Fig. 1. Left side: The strips used in the experiments are cut in such a way that the specimen longitudinal direction, along which the magnetising field **H** is applied and the induction is revealed, forms an angle θ with the parent sheet rolling direction (RD). The transverse direction (TD) is also indicated. Right side: The measured $J_∥$ and $J_⊥$ (solid arrows), together with the polarisations (referred to the whole sample volume) J_{180} and J_{90}, generated by the 180° and 90° phases (dashed arrows), are depicted [see Eq. (A.1)].

reproduce the static and dynamic loss figures at intermediate angles (15° ⩽ θ ⩽ 75°) from the data obtained in the RD and TD directions only.

Instrumental to the formulation of the theoretical model is the combination of the magnetic measurements with the direct observation of the 180° and 90° domain wall (dw) processes by Kerr microscopy.

2. Loss modeling

2.1. Quasi-static energy loss

Our investigation starts from the phenomenological approach worked out in [14,19,21,22], which has demonstrated its validity in assessing the whole magnetic behaviour under quasi-static limit. In this model, the description of the magnetisation process in GO steels takes advantage of the good knowledge of the domain structure and its evolution with the applied field **H**. With high-permeability sheets we can actually simplify the problem by adopting the single crystal approximation and look at the magnetisation process with reference to the Néel's phases and their evolution [13].

By considering then the {110}⟨001⟩ high permeability Goss-textured laminations, we shall identify (Fig. 1) RD (θ = 0°) and TD (θ = 90°) with the [001] and [1$\bar{1}$0] axes of the single crystal, respectively. The strips cut along RD and TD will become the building blocks of the model. Whatever θ, the domain structure in the demagnetised state takes the familiar pattern of anti-parallel domains with the polarisation ± J_s aligned with RD (Fig. 2a, and left side of 2b).

We shall assume that when θ = 0°, a one-dimensional process operates, the magnetisation reversal proceeding exclusively through the displacement of a regular pattern of rigid 180° dws, aligned with **H** (Mode I: two 180° phases). This configuration is called in the following "*180° phase*" (Fig. 2a).

When θ = 90°, the magnetisation process reveals its vector nature. The antiparallel [001] directed domains occupy the whole specimen in the demagnetised state only [left side of Fig. 2b)], but, as $H = |H|$ increases, being the 180° dws unable to move, because perpendicular to **H**, the polarisation $J = |J|$ can grow only thanks to a "*phase transformation*" driven by 90° dws, by which the two 180° phases give way to the [100] and [0$\bar{1}$0] phases. This structure, with four coexisting phases (Mode II) will be colloquially addressed as "*90° phase*" in the following. Such a process ends with the new phases seizing the entire sample volume (Fig. 2b, right side) and is eventually completed by the rotation of J_s towards saturation (Mode III, two phases). Neglecting the closure domains, the whole sample will be occupied, at the end of Mode II, by the [100] and [0$\bar{1}$0] domains, with J_s forming a 45° angle with the sample surface. To note that there is no laterally directed
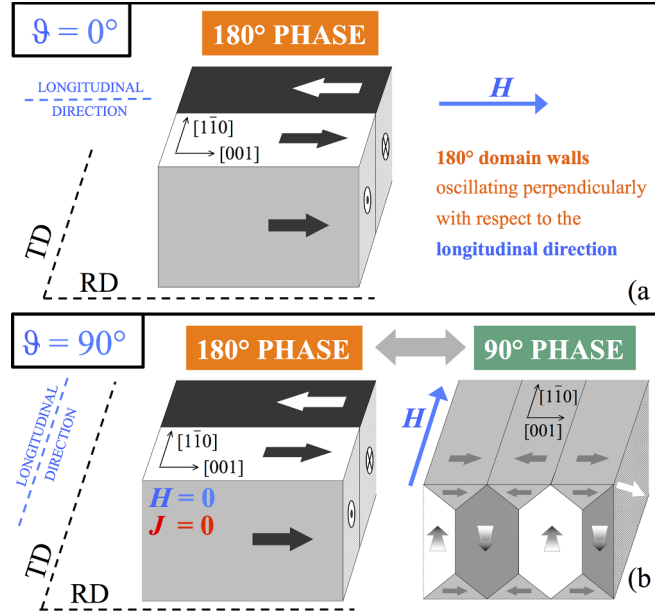

Fig. 2. Domain structure in high-permeability GO sheets, emulating the ideal single-crystal case. Different domain configurations vs. the applied field **H** (parallel to the longitudinal direction, as indicated in Fig. 1) for strips cut along RD (top) and TD (bottom, with the demagnetised state on the left).

macroscopic magnetisation with θ = 0° and θ = 90°. The relationship connecting the 90° phase in-plane polarisation, referred to the whole sample volume (right side of Fig. 1), and its relative volume $v_{90} = V_{90}/V$ (with V_{90} and V the volume of the 90° phase and the sample total volume), turns out to be

$$J_{90} = v_{90}J_s\cos45° = v_{90}\frac{J_s}{\sqrt{2}} \tag{1}$$

In strips cut along directions intermediate between RD and TD, the domain structure observations [14] coupled with the domain theory [10–12] shows that the balance between the two processes discussed above take place in proportions depending on θ. An example of the surface domains evolution vs. the applied field **H** is shown in Fig. 3, for a strip cut at an angle θ = 45° to RD. On passing from $J = 0$ to $J = 0.25$ T, besides the evident 180° dws displacement, a partial 180° phase→ 90° phase transformation can be inferred from the surface
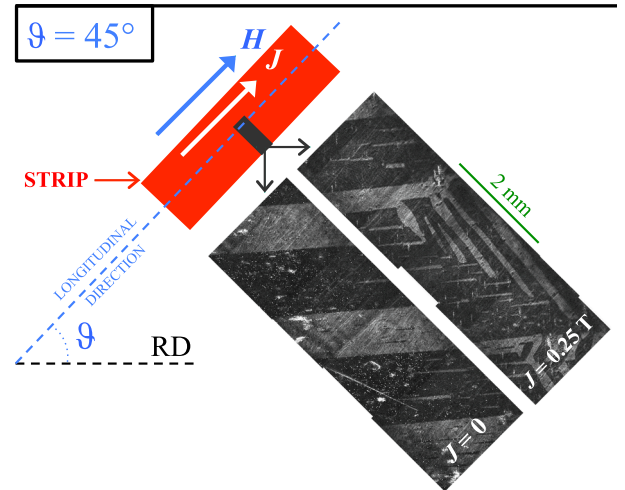
Fig. 3. Surface domain structures, observed by Kerr microscopy, of a strip cut with its longitudinal direction making an angle θ = 45° to RD. Two situations, corresponding to the demagnetised state and $J = 0.25$ T, are reported.

domain structures.

We shall define the polarisation values of the two phases, referred to the whole sample volume, as J_{180} and J_{90}. They are depicted in Fig. 1 (right side), together with the polarisations measured along the longitudinal direction of the strip ($J_\parallel$), and perpendicularly to it ($J_\perp$). We remark that the magnetic properties measured on the RD and TD cut strips have intrinsic character, because, provided the yoke ensures complete flux closure, no demagnetising fields can interfere with the magnetisation process. However, a transverse magnetisation component always appears on strips cut along a generic angle θ and the related demagnetising field will affect, in a way depending on strip width, the magnetisation curve and the loss. Consequently, *the measured properties cannot be assumed as material dependent only*. In this context, the Epstein strips are a subject of specific interest, because they provide, on the one hand, the ubiquitous benchmark of steel sheet testing and, on the other hand, with their 30 mm width, they are subjected to such high lateral demagnetising field that, as discussed in detail in Appendix A, the macroscopic polarisation J is always bound to align with the strip longitudinal direction (that is, with the applied field H). We shall focus in the following on this important case, in particular on the dependence of hysteresis and dynamic losses on θ in a range of measured peak polarisation values (0.15 T $\leqslant J_p \leqslant$ 1.6 T), up to $f =$ 200 Hz.

Considering now the hysteresis energy loss W_{hyst} along the period $T = 1/f$, the model basically assumes its dependence on J_p and θ (ranging from 0° to 90°) to reflect the corresponding domain structure evolution. Consequently, at any θ, W_{hyst} is dissipated through two basic dw mechanisms, concurring to reach the measured peak polarisation.

a) 180° dw displacements inside the 180° phase (of relative volume $v_{180} = 1 - v_{90}$), giving the contribution $J_{180,p}\cos\theta$ to J_p, with $J_{180,p}$ given by Eq. (A.1a) of the Appendix. Let $W_{hyst}^{(180)}[J_{180,p}^{(r)}]$ be the loss corresponding to this process, where

$$J_{180,p}^{(r)} = \frac{1}{v_{180}}J_{180,p} \qquad (2)$$

is the reduced peak polarisation, "*referred*" to v_{180}.

b) 180° phase$\leftrightarrow$90° phase transformation, driven by 90° dws, and giving the contribution $J_{90,p}\sin\theta$ to J_p, with $J_{90,p}$ given by Eq. (A.1b) of the Appendix. Remark that $J_{90,p}$ is connected to the 90° phase volume by Eq. (1).

The total peak polarisation

$$J_p = J_{180,p}\cos\theta + J_{90,p}\sin\theta \qquad (3)$$

is then realised, and, taking advantage of the fact that the net magnetisation transverse to the strip is zero, the total hysteresis loss is obtained after summation of the contributions originated from the *a)* and *b)* mechanisms, weighed through the quantity $\langle v_{180}\rangle_T$, the 180° phase relative volume averaged along T,

$$W_{hyst}(\theta, J_p) = \langle v_{180}\rangle_T W_{hyst}^{(180)}[J_{180,p}^{(r)}] + W_{hyst}^{(90)}[J_{90,p}] \qquad (4)$$

But, as discussed above, two experimentally achievable situations exist where only one of the *a)* or *b)* mechanisms takes place, fulfilled when $\theta = 0°$ and $\theta = 90°$, respectively. Hence

$$W_{hyst}^{(180)}[J_{180,p}^{(r)}] = W_{hyst,EXP}^{(RD)}[J_{180,p}^{(r)}] \qquad (5a)$$

$$W_{hyst}^{(90)}[J_{90,p}] = W_{hyst,EXP}^{(TD)}[J_{90,p}] \qquad (5b)$$

and a relationship relying on pre-emptive knowledge of the magnetic behaviour of the material along RD and TD only, containing no adjustable or arbitrary quantities, can be obtained

$$W_{hyst}(\theta, J_p) = \langle v_{180}\rangle_T W_{hyst,EXP}^{(RD)}[J_{180,p}^{(r)}] + W_{hyst,EXP}^{(TD)}[J_{90,p}] \qquad (6)$$

The evolution of the model parameters $\langle v_{180}\rangle$, $J_{180,p}^{(r)}$, and $J_{90,p}$ vs. θ, for different J_p, is provided in Appendix A.
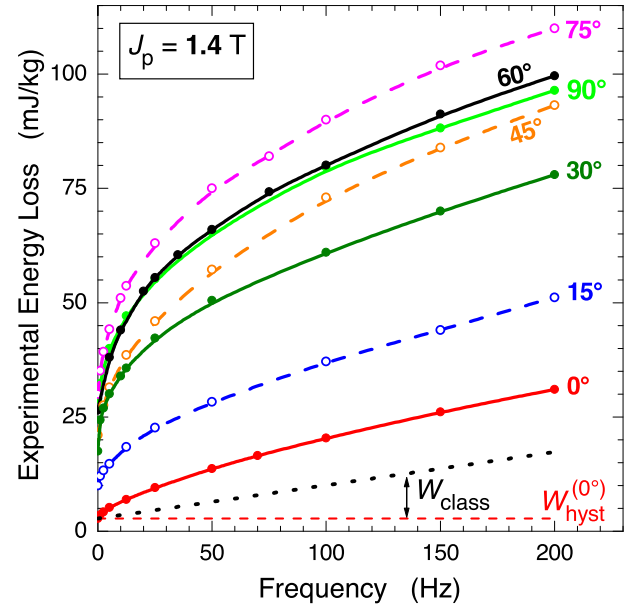

Fig. 4. Energy loss $W(f)$ for peak polarisation $J_p =$ 1.4 T in 0.29 mm thick high-permeability Fe-Si GO Epstein strips cut at various angles θ to the Rolling Direction. The increased non-linearity of $W(f)$ with increasing θ combines with enhanced hysteresis W_{hyst} and excess $W_{exc}(f)$ losses.

2.2. The dynamic losses

The whole phenomenology of the energy loss dependence on J_p and f has found a physically based and well assessed formulation in the statistical Theory of Losses (STL), which provides a rationale for the concept of loss decomposition [20]. This permits us to write the total measured loss W, for any θ, as

$$W(J_p, f) = W_{hyst}(J_p) + W_{class}(J_p, f) + W_{exc}(J_p, f) \qquad (7)$$

where, besides the previously discussed quasi-static term W_{hyst}, obtained by extrapolating $W(f)$ to $f = 0$, we identify the classical W_{class} and the excess W_{exc} components. From Maxwell equations, the following expression for the classical loss per unit volume (independent of θ), in a sheet of conductivity σ and thickness d subjected to sinusoidal induction, is derived

$$W_{class} = \frac{\pi^2}{6}\sigma d J_p^2 f \qquad (8)$$

in the absence of skin effect. The experimental $W_{exc}(J_p, f)$ is then obtained from Eq. (7) by difference.

The example of experimental $W(f)$ behaviours shown in Fig. 4 ($J_p =$ 1.4 T) for θ ranging between 0° and 90°, puts in evidence, besides increasing non-linearity of $W(f)$, sharp and similar increase of W_{hyst} and $W_{exc}(f)$ with rising θ, as shown by the loss decomposition made via Eqs. (7) and (8). In particular, it is found that $W_{exc}(f)$ follows to good approximation a power law dependence on frequency $W_{exc}(f) \propto f^q$, with q decreasing from the usual value $q = 0.5$ for $\theta = 0°$ to $q \cong 0.35$ for $\theta \geqslant 30°$. According to the STL, this decrease of q follows from faster dw multiplication effect with increasing frequency. Quantitatively, this can be expressed in terms of number n of Bertotti's simultaneously reversing magnetic objects, obeying a law of the type $n \sim (H_{exc}/V_0)^m$, with $m > 1$, $H_{exc} = W_{exc}/4J_p$ and V_0 the base statistical parameter accounting for the distribution of the local coercive fields [20]. The calculations show that in such a case $W_{exc}(f) \propto f^{[1/(1+m)]}$.

We shall demonstrate in the following Section how the $W_{hyst}(\theta)$ behaviour can be predicted in terms of the measured intrinsic quantities $W_{hyst,EXP}^{(RD)}$ and $W_{hyst,EXP}^{(TD)}$ by means of Eq. (6). This feat is one important consequence of the very local nature of the dissipation processes (elementary Barkhausen jumps) occurring under quasi-static excitation.
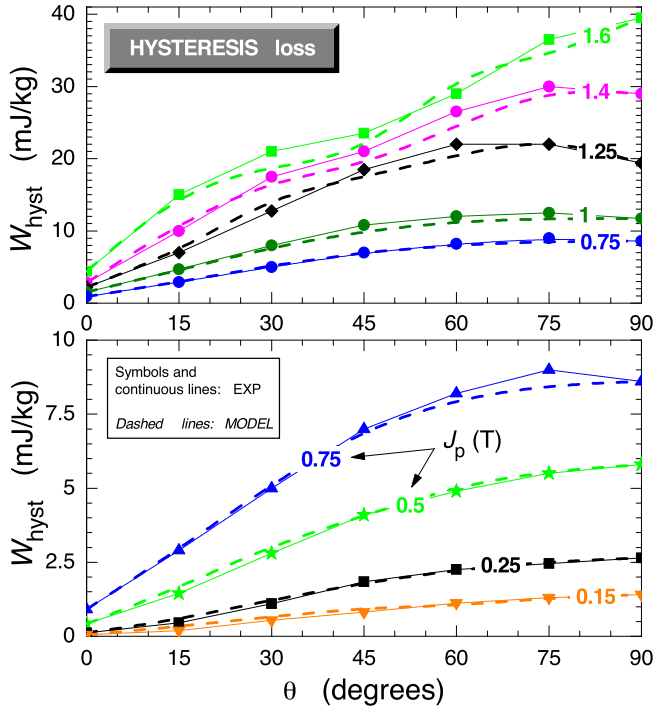
Fig. 5. Behaviour of the hysteresis loss component vs. the cutting angle θ formed by the applied field with RD (see Fig. 1), for high (top) and low (bottom) peak polarisations J_p. The theoretical loss figures at intermediate ($15° \leqslant \theta \leqslant 75°$) cutting angles are obtained after interpolation performed via Eq. (6) of the RD and TD experimental values.

The same property expectedly applies, though on a larger scale (that of the domain wall and its immediate surroundings), when considering the eddy current mechanisms responsible for W_{exc}, which is, in addiction, correlated to W_{hyst} via the statistics of coercivities. Finally, we have experimentally verified, under quasi-static and dynamic regimes, the boundary conditions $J_\| = J$ and $J_\perp = 0$ [Eq. (A.2)], with ensuing frequency-independent model parameters $\langle v_{180} \rangle$, $J_{180,p}^{(r)}$, and $J_{90,p}$. For all these reasons, it appears justified to apply a same conceptual scheme in the approach to the behaviour of W_{hyst} and W_{exc} as a function of θ, and consequently write

$$W_{exc}(\theta, J_p) = \langle v_{180} \rangle_T W_{exc,EXP}^{(RD)}[J_{180,p}^{(r)}] + W_{exc,EXP}^{(TD)}[J_{90,p}] \quad (9)$$

where for the RD and TD excess components, relationships analogous to 5(a) and (5b) hold.

3. Experimental, results and discussion

We have investigated a high-permeability GO Fe-(3 wt%) Si alloy (Nippon Steel M2H), with average grain size of 1–2 cm. This material, with its maximum crystal deviation of about 3° of the [001] axis with respect to RD, best emulates the ideal condition represented by the monocrystal. Epstein strips (300 mm long, 30 mm wide) were cut from a 0.29 mm thick parent sheet (Fig. 1), along directions θ ranging between RD and TD at 15° intervals. Magnetic testing was carried out by means of a single sheet tester, making use of a double-C laminated yoke (125 mm × 30 mm cross-section) with pole faces at a distance of 240 mm, and air-flux compensation automatically achieved by means of a mutual inductor.

The magnetising field is known by measuring the exciting current, after determination of the magnetic path length by comparative tests with an Epstein frame, whereas the induction is detected by means of a
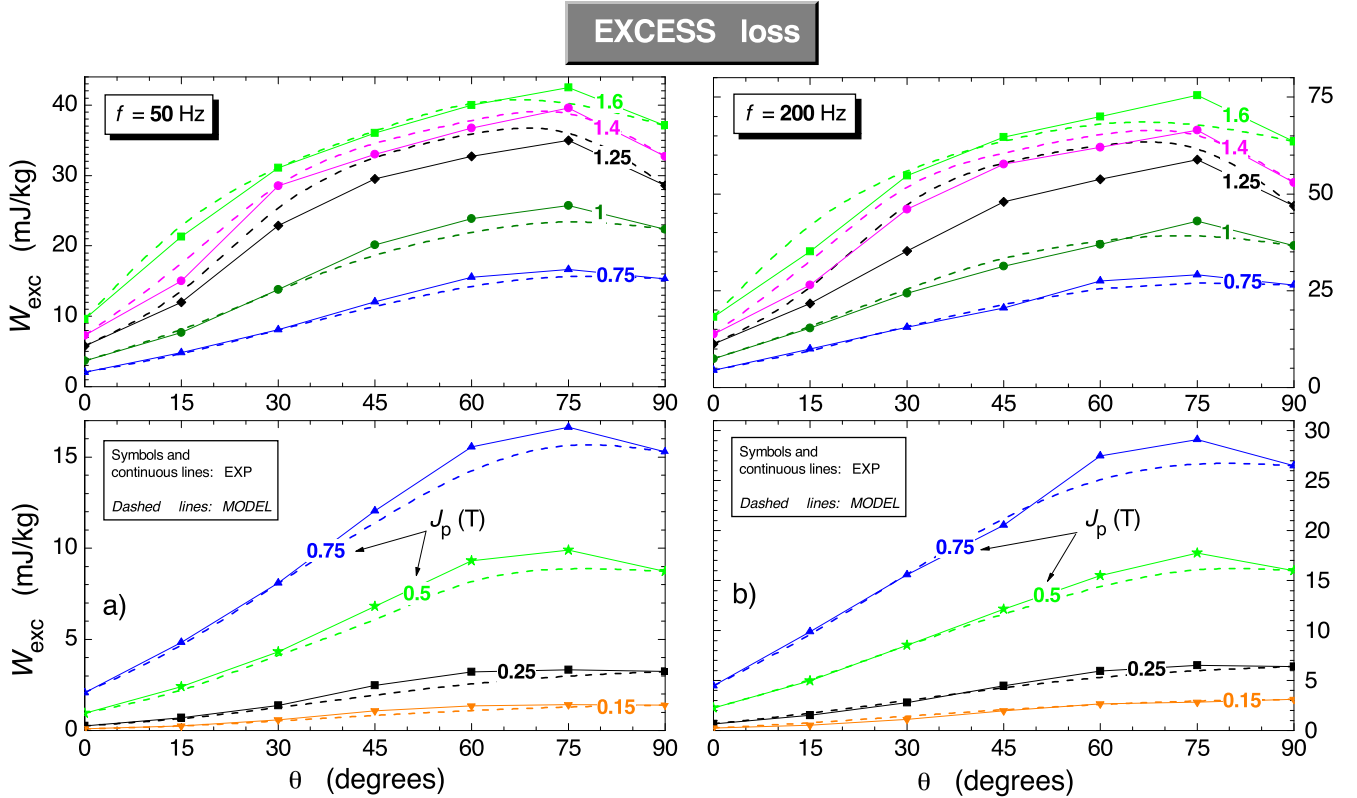

Fig. 6. Behaviour of the excess loss component vs. the cutting angle θ formed by the applied field with RD (see Fig. 1), for low (bottom section) and high (top section) peak polarisations J_p, at $f = 50$ Hz (a) and $f = 200$ Hz (b). The theoretical loss figures at intermediate ($15° \leqslant \theta \leqslant 75°$) cutting angles are obtained after interpolation performed via Eq. (9) of the RD and TD experimental values.
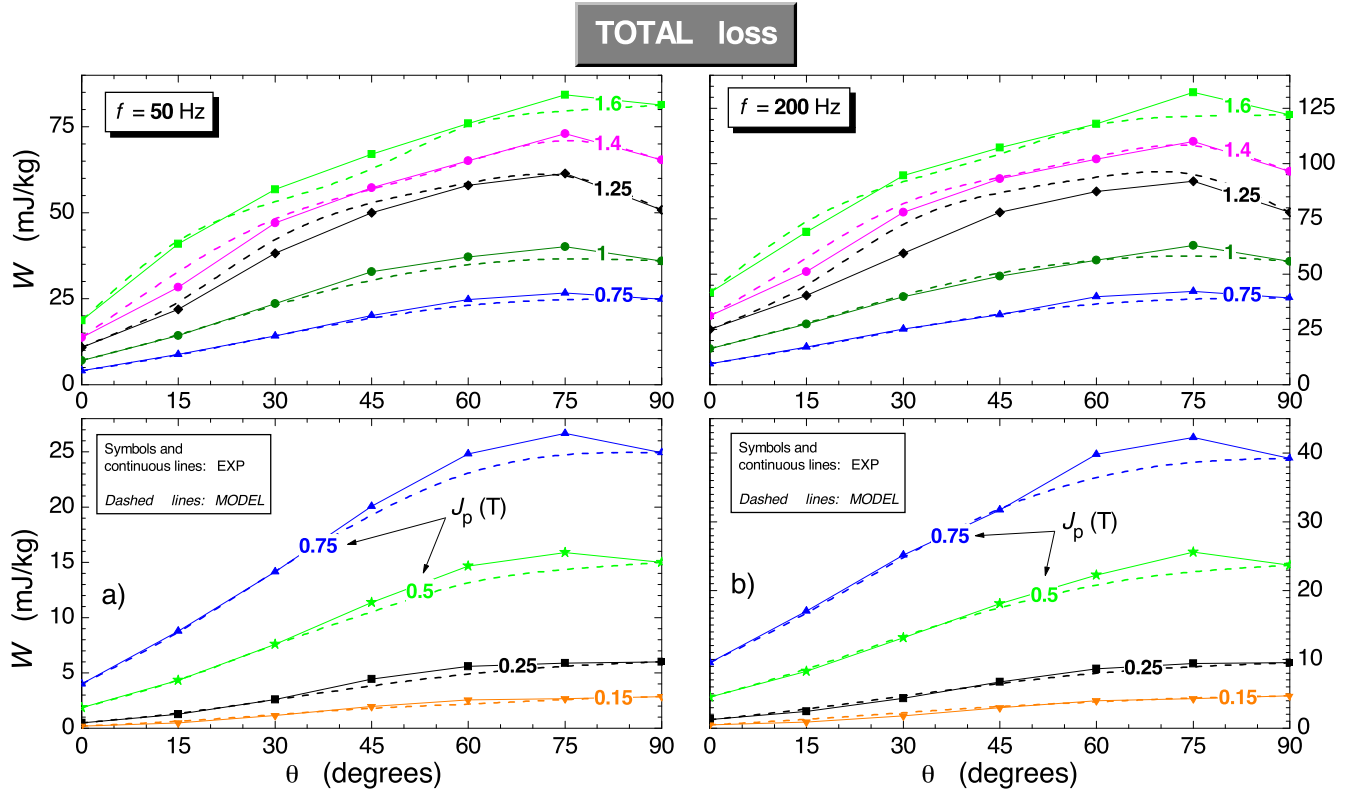
Fig. 7. Behaviour of the total loss vs. the cutting angle θ formed by the applied field with RD (see Fig. 1), for low (bottom section) and high (top section) peak polarisations J_p, at $f = 50$ Hz (a) and $f = 200$ Hz (b). The theoretical loss figures are obtained from Eqs. (6)–(9).

few-turn coil wound around the strip.

Hysteresis loops and losses have been measured, under sinusoidal controlled induction waveform, in the peak induction interval 0.15 T ≤ J_p ≤ 1.6 T, with the frequency f ranging between 1 and 200 Hz.

The measured energy loss per cycle has been subjected to the loss separation procedure (Section 2.2), and the found values of the hysteresis and excess (at $f = 50$ Hz and $f = 200$ Hz) loss components are shown in Figs. 5 and 6, respectively. In the 15° ≤ θ ≤ 75° range, these figures have been satisfactorily reproduced by means of Eq. (6) for W_{hyst} and Eq. (9) for W_{exc}. The theoretical total loss W, obtained by means of Eq. (7), summing up the classical term [Eq. (8)] and the calculated W_{hyst} and W_{exc} components, is compared to the experimental one in Fig. 7, in the same θ range.

The performance of the model can be quantified introducing, for all loss components, the relative difference $\eta = |W^{(MODEL)} - W^{(EXP)}|/W^{(EXP)}$. This quantity, of the order of few percent in most cases, reaches its maximum around $\theta = 45°$. For W_{hyst}, one gets $\eta_{max} \cong 13\%$ when $J_p \geqslant 1.5$ T, whereas for W_{exc}, $\eta_{max} \cong 22\%$ at $J_p = 1.25$ T. These discrepancies can be ascribed to the idealised nature of the model, which, based on the single crystal approximation, does not take into consideration the whole domain structure, in particular the surface domains.

Finally, it must be remarked that the disagreements between the experimental and theoretical values of W_{hyst} and W_{exc} are significantly shadowed ($\eta_{max} \cong 12\%$ at $J_p = 1.25$ T and $f = 200$ Hz) when considering the total loss W, the important quantity from the practical viewpoint.

4. Conclusions

We have shown that the magnetic losses of high-permeability grain-oriented Fe-Si sheets, measured up to 200 Hz on Epstein strips cut at angles θ to the rolling direction ranging from 0° to 90°, can be assessed by means of the loss decomposition method, in conjunction with a phenomenological model of the magnetisation process and its evolution with the cutting angle. Such a model is based on the appraisal of the correlated roles of the 180° dws displacements and the 90° transitions, giving rise to a defined macroscopic magnetic behaviour of the steel sheet along the direction defined by θ. In the specific case of Epstein strips, the relative contributions of the 180° and 90° domain wall processes to magnetisation process, hysteresis W_{hyst}, and excess $W_{exc}(f)$ losses, balanced in such a way as to always provide, according to the experiments, zero net magnetisation across the strip, are obtained by linear combination of the same quantities measured on the strips cut along RD and TD, respectively. This amounts to assume that, up to the frequencies where the skin effect eventually sets in, we are able to predict the fractional volumes v_{180} and v_{90} occupied at each instant of time by the 180° and 90° processes and that such volumes negligibly depend on frequency.

It is then observed that on the whole 15° ≤ θ ≤ 75° investigated range both $W_{hyst}(J_p)$ and $W_{exc}(J_p, f)$ [and, ultimately, the total loss $W(J_p, f) = W_{hyst}(J_p) + W_{class}(J_p, f) + W_{exc}(J_p, f)$] are satisfactorily predicted, across the wide J_p interval 0.15 T ÷ 1.6 T, by a simple linear model involving the corresponding RD and TD quantities, without any adjusting parameters.

Declaration of Competing Interest

The authors declare that they have no known competing financial interests or personal relationships that could have appeared to influence the work reported in this paper.

Appendix A. Behaviour vs. θ and J_p of the model parameters $\langle v_{180} \rangle_T$, $J_{180,p}^{(r)}$, and $J_{90,p}$

In the strip plane, the polarisation components (referred to the whole sample volume) parallel and perpendicular to its longitudinal direction, are (see right side of Fig. 1)

$$J_{\parallel} = J_{180}\cos\theta + J_{90}\sin\theta \tag{A.1a}$$

$$J_{\perp} = J_{180}\sin\theta - J_{90}\cos\theta \tag{A.1b}$$

When considering an Epstein strip, thanks to a large in-plane demagnetising field perpendicular to the longitudinal direction, we have [14]

$$J_{\parallel} = J \tag{A.2a}$$

$$J_{\perp} = 0 \tag{A.2b}$$

These relationships, together with the Eq. (A.1), give

$$J_{180} = J\cos\theta \tag{A.3a}$$

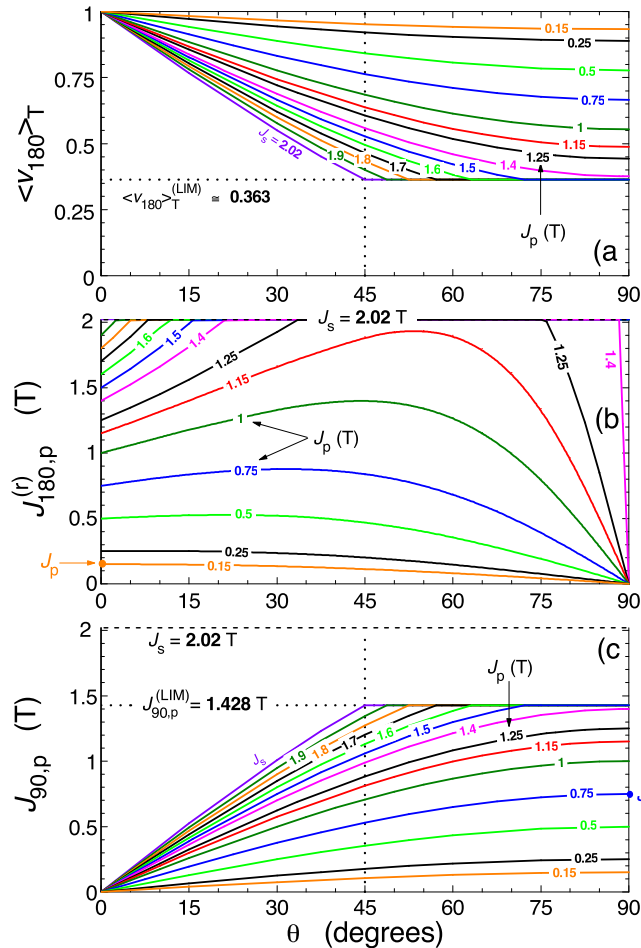$$J_{90} = J\sin\theta \tag{A.3b}$$

The peak value in the 90° phase

$$J_{90,p} = J_p\sin\theta \tag{A.4}$$

is shown in Fig. 8 (c), with its upper value

$$J_{90,p}^{(LIM)} = \frac{J_s}{\sqrt{2}} \cong 1.428 \text{ T} \tag{A.5}$$

obtained from Eq. (1) for $v_{90} = 1$.

Considering now the 180° phase, and making explicit the time dependence, the peak value of polarisation referred to the volume fraction v_{180} [Eq. (2)] is, from Eq. (A.3a),

Fig. 8. Behaviour, vs. the angle θ formed by the applied field with RD, of the model parameters $\langle v_{180} \rangle_T$, limited by the lower threshold $\langle v_{180} \rangle_T^{(LIM)}$ (a), $J_{180,p}^{(r)}$ (b), and $J_{90,p}$, limited by the upper threshold $J_{90,p}^{(LIM)}$ (c).

$$J_{180,p}^{(r)} = \left[\frac{J(t)}{v_{180}(t)} \right]_p \cos\theta \tag{A.6}$$

With the volume fraction [from Eqs. (1) and (A.3b)]

$$v_{180}(t) \equiv 1 - v_{90}(t) = 1 - \sqrt{2}\frac{|J(t)|}{J_s}\sin\theta \tag{A.7}$$

the relationship (A.6) becomes

$$J_{180,p}^{(r)} = \left[\frac{J(t)}{1 - \sqrt{2}\frac{|J(t)|}{J_s}\sin\theta} \right]_p \cos\theta \tag{A.8}$$

From Eq. (A.7) one also gets v_{180} averaged over the period T

$$\langle v_{180} \rangle_T = 1 - \sqrt{2}\frac{1}{J_s}\langle |J(t)| \rangle_T \sin\theta \tag{A.9}$$

Under sinusoidal induction (with $\omega = 2\pi f$)

$$J(t) = J_p\cos\omega t \tag{A.10}$$

Eq. (A.8) provides, when $t = 0$ [see Fig. 8 (b)],

$$J_{180,p}^{(r)} = \frac{J_p}{1 - \sqrt{2}\frac{J_p}{J_s}\sin\theta}\cos\theta \tag{A.11}$$

and Eq. (A.9) becomes

$$\langle v_{180} \rangle_T = 1 - \frac{2\sqrt{2}}{\pi}\frac{J_p}{J_s}\sin\theta \tag{A.12}$$

shown in Fig. 8 (a), where its lower limit

$$\langle v_{180} \rangle_T^{(LIM)} = 1 - \frac{2}{\pi} \cong 0.363 \text{ T} \tag{A.13}$$

also appears.

References

[1] F. Fiorillo, G. Bertotti, C. Appino, M. Pasquale, Soft magnetic materials, in: M. Peterca (Ed.), Wiley Encyclopedia of Electrical and Electronics Engineering, John Wiley and Sons, Inc., Hoboken, New Jersey, 2016, pp. 1–42, , https://doi.org/10.1002/047134608X.

[2] F. Marketos, D. Marnay, T. Ngnegueu, IEEE Trans. Magn. 48 (2012) 1677–1680, https://doi.org/10.1109/TMAG.2011.2173667.

[3] S. Magdaleno-Adame, T.D. Kefalas, A. Fakhravar, J.C. Olivares-Galvan, in: 2018 IEEE International Autumn Meeting on Power, Electronics and Computing (ROPEC 2018), Ixtapa, Mexico.

[4] S. Lopez, B. Cassoret, J.F. Brudny, L. Lefebvre, J.N. Vincent, IEEE Trans. Magn. 45 (2009) 4161–4164, https://doi.org/10.1109/TMAG.2009.2023243.

[5] J. Maraví-Nieto, Z. Azar, A.S. Thomas, Zi-Qiang Zhu, J. Eng. 2019 (2019) 3682–3686, https://doi.org/10.1049/joe.2018.8171.

[6] C. Appino, C. Ragusa, F. Fiorillo, Int. J. Appl. Electromagn. Mech. 44 (2014) 355–370, https://doi.org/10.3233/JAE-141798?.

[7] E. Cardelli, A. Faba, JAP 115 (2014) 17A327, https://doi.org/10.1063/1.4865772.

[8] A. Furuya, J. Fujisaki, Y. Uehara, K. Shimizu, H. Oshima, T. Matsuo, IEEE Trans. Magn. 50 (2014) 7300604, https://doi.org/10.1109/TMAG.2014.2329679.

[9] A.P.S. Baghel, A. Gupta, K. Chwastek, S.V. Kulkarni, Physica B 462 (2015) 86–92, https://doi.org/10.1016/j.physb.2015.01.026.

[10] A. Hubert, R. Schäfer, Magnetic Domains: The Analysis of Magnetic Microstructures, Springer, New York, 3-540-64108-4, 1998.

[11] S. Shin, R. Schaefer, B.C. DeCooman, JAP 109 (2011) 07A307, https://doi.org/10.1063/1.3535547.

[12] R. Schäfer, I. Soldatov, S. Arai, JMMM 474 (2019) 221–235, https://doi.org/10.1016/j.jmmm.2018.10.100.

[13] L. Néel, J. Phys. Radium 5 (1944) 241–251.

[14] F. Fiorillo, L.R. Dupré, C. Appino, A.M. Rietto, IEEE Trans. Magn. 38 (2002) 1467–1475, https://doi.org/10.1109/20.999119.

[15] S. Yue, Y. Li, Q. Yang, K. Zhang, C. Zhang, IEEE Trans. Magn. 55 (2019), https://doi.org/10.1109/TMAG.2019.2895152.

[16] W.A. Pluta, IEEE Trans. Magn. 52 (2016) 6300912, https://doi.org/10.1109/TMAG.2015.2496547.

[17] M.A. Bahmani, E. Agheb, T. Thiringer, H.K. Høidalen, Y. Serdyuk, J. Renew. Sustain. Energy 4 (2012) 033112, , https://doi.org/10.1063/1.4727910.

[18] M.A. Bahmani, E. Agheb, T. Thiringer, H.K. Høidalen, Y. Serdyuk, J. Renew. Sustain. Energy 4 (2012) 033113, , https://doi.org/10.1063/1.4727917.

[19] F. Fiorillo, C. Appino, C. Beatrice, F. Garsia, JMMM 242–245 (2002) 257–260, https://doi.org/10.1016/S0304-8853(01)01271-9.

[20] G. Bertotti, Hysteresis in Magnetism, Academic Press, New York, 1998 0-12-093270-9..

[21] L.R. Dupré, F. Fiorillo, J. Melkebeek, A.M. Rietto, C. Appino, JMMM 215–216 (2000) 112–114, https://doi.org/10.1016/S0304-8853(00)00088-3.

[22] L.R. Dupré, F. Fiorillo, C. Appino, A.M. Rietto, J. Melkebeek, JAP 87 (2000) 6511–6513, https://doi.org/10.1063/1.372754.